

# Self-Powered Multifunction Ionic Skins Based on Gradient Polyelectrolyte Hydrogels

Mingyang Xia,<sup>§</sup> Na Pan,<sup>§</sup> Chao Zhang, Chengjing Zhang, Wenxin Fan,\* Yanzhi Xia, Zuankai Wang,\* and Kunyan Sui\*



Cite This: <https://doi.org/10.1021/acsnano.1c11505>



Read Online

ACCESS |

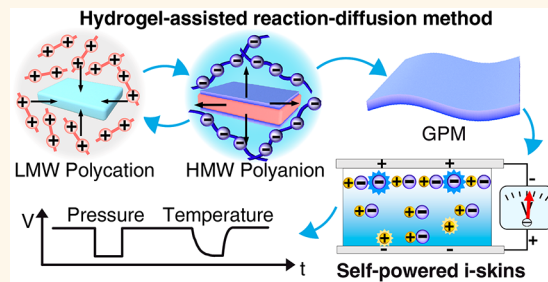
Metrics & More

Article Recommendations

Supporting Information

**ABSTRACT:** Human skin is the largest organ, and it can transform multiple external stimuli into the biopotential signals by virtue of ions as information carriers. Ionic skins (*i*-skins) that can mimic human skin have been extensively explored; however, the limited sensing capacities as well as the need of an extra power supply significantly restrict their broad applications. Herein, we develop self-powered humanlike *i*-skins based on gradient polyelectrolyte membranes (GPMs) that can directly and accurately perceive multiple stimuli. Prepared by a hydrogel-assisted reaction-diffusion method, the GPMs exhibit gradient-distributed charged groups across polymer networks, enabling one to generate a thickness-dependent and thermoresponsive self-induced potential in a hydrated situation and in a humidity-sensitive self-induced potential in a dehydrated/dried situation, respectively. Consequently, the GPM-based *i*-skins can precisely detect pressure, temperature, and humidity in a self-powered manner. The coupling of mechano-electric and thermo-electric effects inherent in GPMs provides a general strategy for developing innovative self-powered ion-based perception systems.

**KEYWORDS:** ionic skins, gradient polyelectrolyte membranes, self-induced potential, multifunction sensors, reaction-diffusion



Skin is a physical barrier for human beings, and it also serves as a multiple sensor capable of perceiving multiple stimuli (e.g., pressure, temperature, humidity, etc.) and communicating with the surrounding environment. The perception ability of human skin stems from ubiquitous receptors in it, which can encode the external stimuli into recognizable biopotential signals.<sup>1–3</sup> In the past decade, considerable efforts have been made to develop artificial skins to mimic the properties of human skin for potential applications in artificial intelligence, soft robotics, prosthetics, personal healthcare, and the Internet of Things.<sup>4–10</sup> Among others, ionic skins (*i*-skins) have attracted tremendous interest owing to many inherent advantages such as humanlike signal carriers (i.e., ions), tissue-like mechanical properties, good biocompatibility, high stretchability, and transparency.<sup>11–13</sup> Currently, various piezoresistive, capacitive, or iontronic *i*-skins have shown improved detection sensitivity<sup>14,15</sup> and limit,<sup>16,17</sup> multiple perception ability,<sup>18–20</sup> and superior mechanical properties;<sup>21–23</sup> however, the practical application of them remains challenging. One major limitation lies in the inevitable need of the bulky and external alternating current power supply (Figure 1a),<sup>21–26</sup> which undercuts the light weight and compactness of wearable devices.

Designing self-powered skins that can directly harvest the environmental energy is a promising way to circumvent extra

power supplies.<sup>27</sup> Conventional triboelectric or piezoelectric nanogenerators are capable of constructing self-powered electronic skins,<sup>28–33</sup> but they are not suitable for the fabrication of self-powered *i*-skins or for detecting low-frequency and static mechanical stimuli. Recently, flexible ionic diodes consisting of a pair of polycation and polyanion conductors have shown great potential as self-powered *i*-skins capable of recognizing low-frequency/static mechanical stimuli.<sup>34–36</sup> However, such ionic diode-based devices suffer from certain limitations such as the unwanted delamination between diode components, a single pressure-sensing function, and an unclear mechanolectric conversion mechanism.

Distinct from diode-based devices, our work is based on a gradient polyelectrolyte membrane (GPM), an interesting material widely used in electrodialysis, ionic rectification, and osmotic energy collection owing to its selective and unidirectional permeation of anions or cations.<sup>37–40</sup> The self-induced

Received: December 25, 2021

Accepted: February 17, 2022

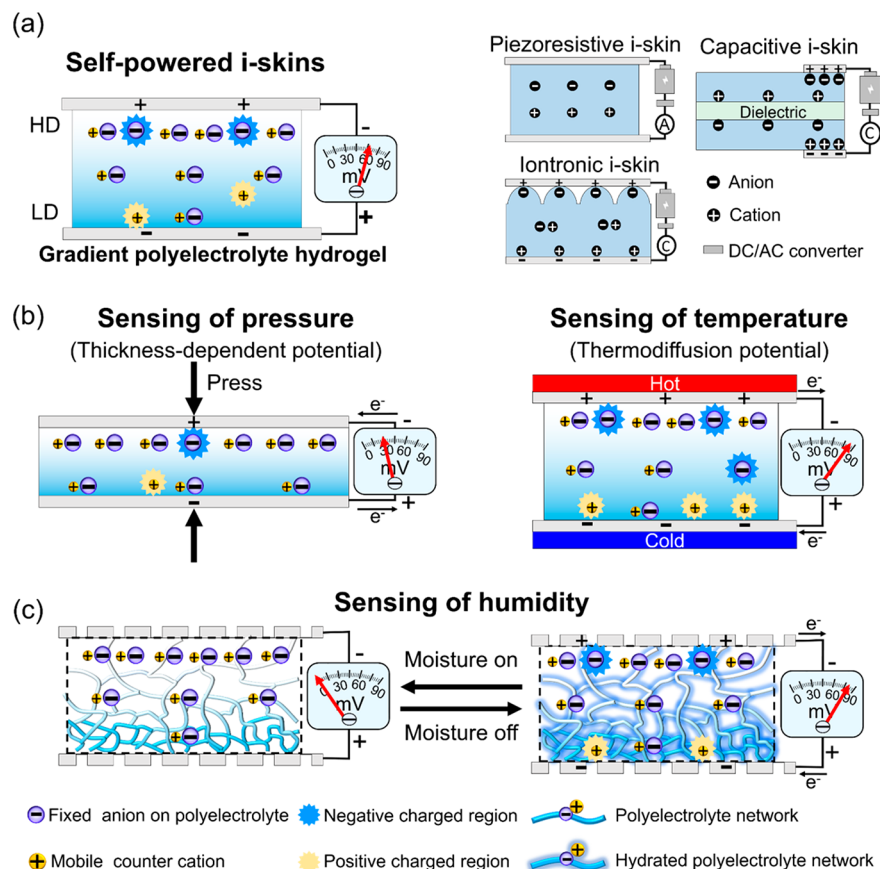


**Figure 1.** Schematic illustrations of traditional i-skins and GPM-based self-powered i-skins. (a) Traditional piezoresistive, capacitive, and iontronic i-skins. (b) Pressure- and temperature-sensing mechanisms of GPM-based self-powered i-skins. (c) Humidity-sensing mechanism of self-powered i-skins.

potential of gradient ionic membrane has been demonstrated to be highly associated with the gradient distribution of charged groups and the diffusion capability of counterions as well as the environmental moisture.<sup>41–43</sup> Leveraging these features, here we demonstrate the feasibility of using GPMs as the self-powered i-skins for the precise perception of multiple stimuli (Figure 1b,c). Prepared by a hydrogel-assisted reaction-diffusion, the GPMs exhibit a thickness-dependent and thermoresponsive self-induced potential in a hydrated situation and a humidity-sensitive self-induced transmembrane potential in a dehydrated/dried situation. Therefore, the resulting GPM-based self-powered i-skins can reliably and precisely detect external pressure, temperature, and humidity stimuli. In particular, we revealed the mechanoelectric conversion/sensing mechanisms of GPM-based/ionic diode-based self-powered i-skins. It has been demonstrated that the mechanoelectric conversion of GPM/ionic diode-based self-powered devices originates from the thickness-dependent self-induced potentials of GPMs/ionic diodes (Mechanism I) and/or varying voltage losses at the electrode/GPM (or electrode/diode) interfaces (Mechanism II) in response to pressure. This work develops a versatile strategy for constructing multifunction self-powered i-skins and will find numerous applications, especially in scenarios where multiple sensing is needed yet access to power is otherwise impossible.

## RESULTS AND DISCUSSION

### Preparation and Characterization of Hydrogel-Based GPMs.

The hydrogel-based GPMs were prepared by

hydrogel-assisted reaction-diffusion method (Figure 2a). In brief, a pure polyacrylamide (PAM) hydrogel was first submerged into a concentrated low-molecular-weight (LMW) polycation solution for the formation of a polycation-rich hydrogel container based on the concentration gradient-induced diffusion. Thereafter, the LMW polycation-rich hydrogel container was immersed into a high-molecular-weight (HMW) polyanion solution with a low concentration. Once the LMW polycation-rich hydrogel container contacted the HMW polyanion solution, a thin complex layer formed instantly on the surface of the hydrogel due to the diffusion of LMW polycation into the polyanion solution and the strong electrostatic complexation between them. As the LMW polycation within the hydrogel container gradually diffused across the complex layer and interacted with the polyanion, the thickness of the membrane gradually grew (Figure 2a). For the as-prepared GPMs, the LMW polycations (i.e., stationary anions) are gradient-distributed, because the HMW polyanions at the side close to the polycation-rich hydrogel container (denoted as the LD side) can react with more LMW polycations than that of the other side (denoted as HD side), as shown in Figure 2a.<sup>44,45</sup> In consequence, the high density of LMW polycations at the LD side of GPMs can consume more negatively charged groups (i.e., stationary anions) on polyanions due to the formation of electrostatic complexation between them, leading to the lower density of residual negative charges at the LD side compared to that of the HD side. By the meticulous control of the molecular weight (Mw), concentration, and type of polyelectrolyte, the

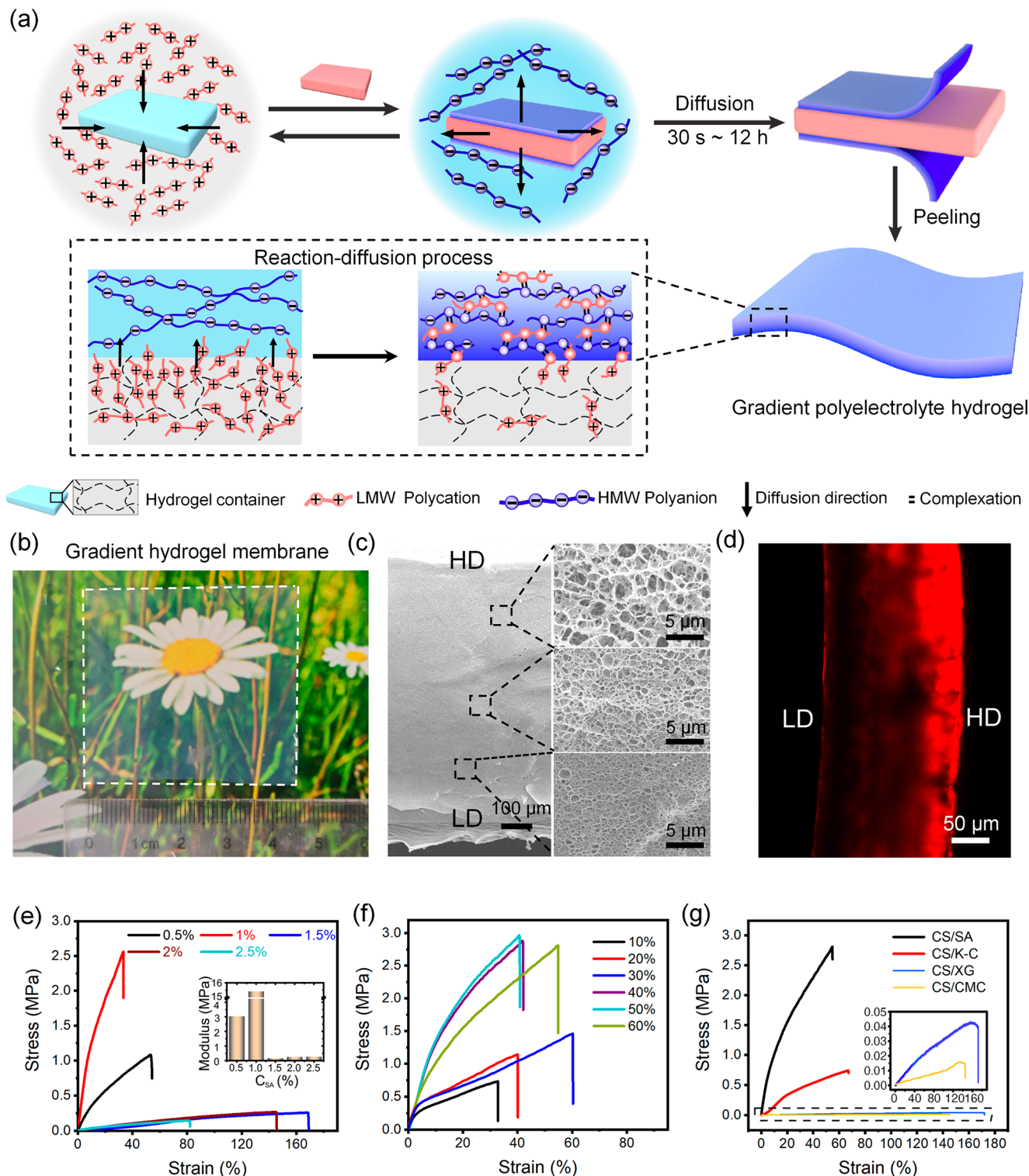


**Figure 2. Preparation and characterization of GPMs.** (a) Synthesis mechanism of hydrogel-based GPMs. (b) Optical images of hydrogel-based CS/SA GPM. (c, d) SEM images (c) and CLSM image (d) showing the cross-section views of CS/SA GPMs. (e, f) Tensile strength of hydrogel-based CS/SA GPMs prepared with different SA concentrations (e) and CS concentrations (f). The inset of (e) is the modulus of membranes. (g) Tensile strength of GPMs prepared with different HMW polyanions. The inset of (g) is the stress–strain curves of CS/XG and CS/CMC GPMs.

hydrogel-based GPMs can gain a highly tunable charge gradient and mechanical property.<sup>46–49</sup>

As a proof of concept, when the 40 wt % chitosan (CS, Mw = 5000) and 1 wt % sodium alginate (SA, Mw = 388 000) were used as the LMW polycation and HMW polyanion solution,

respectively, a transparent gradient CS/SA hydrogel membrane formed directly on the surface of hydrogel containers (Figure 2b and Figure S1). The electrostatic complexation between SA and CS can be confirmed by two new peaks that appeared at 1726 and 1522 cm<sup>-1</sup> in the Fourier transform infrared (FTIR)

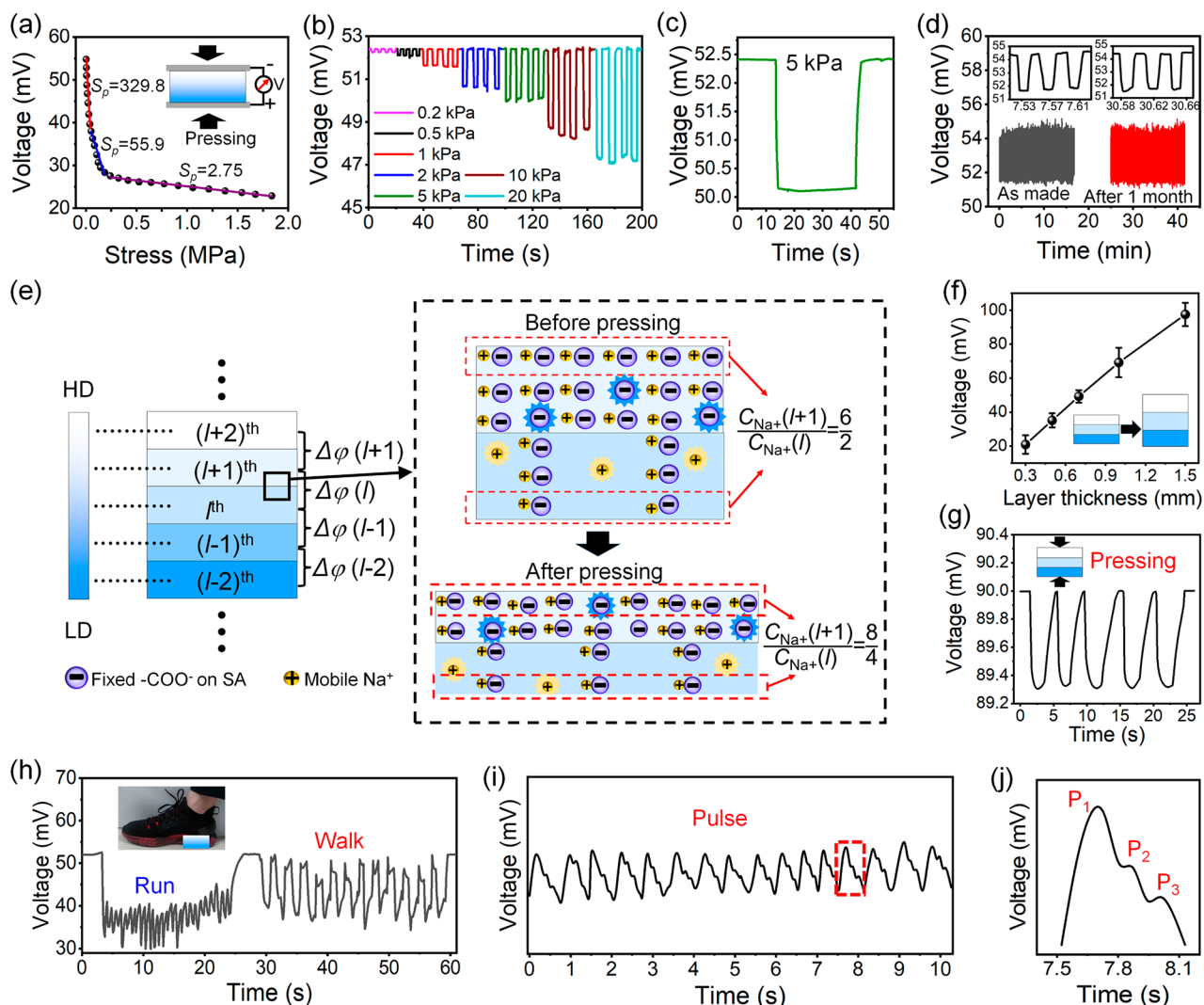


**Figure 3.** Pressure-sensing performance and mechanism of GPM-based self-powered i-skins. (a–d) Output voltage of self-powered i-skins under different conditions: (a) under a gradually increased pressure, (b) under different low-frequency pressures (~0.2 Hz), (c) under a static pressure, and (d) under repeated loading/unloading of 5 kPa pressure of 500 cycles. Two signals in (d) were obtained by the same self-powered i-skin encapsulated into VHB tapes before and after storage in the atmosphere for 1 month. (e) Schematic illustration of pressure-sensing mechanism of self-powered i-skin. (f) Output voltage of asymmetric PAM/SA hydrogels consisting of three-layer homogeneous PAM/SA hydrogels with different SA concentrations. (g) Output voltage of asymmetric PAM/SA hydrogel under a repeated 2 kPa pressure. (h–j) Output voltage of self-powered i-skins in response to (h) walking and running motions, and (i, j) a human pulse. The insets in (h) show the sensor adhered onto the heel.

spectrum of CS/SA membranes (Figure S2).<sup>45,46</sup> Figure 2c shows that the CS/SA hydrogel membrane possesses a gradient pore structure from the HD side to the LD side, originating from the gradient electrostatic complexation. The pores are interpenetrating with widely distributed diameters (~5 nm to 10  $\mu\text{m}$ , Figure S3), beneficial for the ion transport within GPMs.<sup>50</sup> Compared to the LD side, the HD side possesses much larger pores because of the low electrostatic complexation density for forming a loose cross-linking network, as evidenced by the lower nitrogen content in the HD side (i.e., low LMW CS content) (Figure S4a).

This gradient feature can be also reflected by investigating the charge density distribution of the CS/SA hydrogel membrane. It can be seen from Figure S4 that the LD side of CS/SA GPMs possesses a higher nitrogen content (i.e., higher CS content) than the HD side. The molar ratios of  $-\text{COONa}$  on SA to  $-\text{NH}_2$  on CS are estimated to be 1.82 and

1.23, respectively, indicating that the GPMs are negatively charged throughout the thickness direction and hold the gradient-distributed net negative charges along the thickness direction (Figure S5). Such a distinct charge gradient of the CS/SA GPMs can be visually validated by the results of confocal laser scanning microscopy (CLSM) (Figure 2d). Before the CLSM characterization, the CS/SA GPMs were dyed by the dilute solution of positively charged rhodamine 6G ( $10^{-6}$  M), which would be absorbed on the negatively charged groups within GPMs. Clearly, the rhodamine 6G (red fluorescence) is gradient-distributed, further manifesting the gradient-distributed residual negative charges within GPMs. In addition to the gradient pore structure and charge densities, the CS/SA membranes also display a fine-tunable thickness from 0.05 to 1.2 mm by easily adjusting the reaction time (Figure S6) as well as well modulated morphologies by designing surface patterns of the hydrogel containers (Figure

S7). Notably, the CS/SA GPMs encapsulated into 3M VHB tapes maintained the stable voltage output after storage in the air for ~150 d and presented similar microstructures between the samples before and after storage for ~150 d (Figure 2c and Figure S8). This suggests that the LMW CS with multiple ionogenic groups complexed with polyanions can hardly move in the GPMs.

We then investigated the mechanical properties of gradient CS/SA hydrogel membranes, an important parameter for practical applications especially in artificial ionic skins. As shown in Figure 2e,f, both the tensile strength and elastic modulus of CS/SA GPMs have an obvious improvement with increasing concentration of SA from 0.5 to 1 wt % because of the enhanced electrostatic complexation density. The further increase of SA concentration caused the decrease of tensile strength and elastic modulus (Figure 2e). This is because an excessively dense polyelectrolyte complex membrane quickly forms on the surface of a PAM hydrogel container, which in turn hinders the diffusion of CS and eventually leads to the formation of a very loose and weak polyelectrolyte complexation layer on the HD side of the as-prepared membranes (Figure S9). Analogous to SA, the increase of LWM CS concentration could also improve the mechanical properties of the membranes. Notably, when the CS concentration increased over 40 wt %, the further increase of CS concentration had little influence on the mechanical properties of the resulting GPMs. Moreover, we also constructed the CS/SA GPMs using different molecular weights of CS and SA. Here, the CS with the molecular weights of 2000, 5000, and 7000 were used and denoted as CS<sub>2000</sub>, CS<sub>5000</sub>, and CS<sub>7000</sub>, respectively. When the CS<sub>2000</sub> was utilized, the resulting CS/SA GPM presented a low modulus and tensile strength due to the relatively weaker electrostatic binding between CS and SA (Figure S10a). Similar to the case of high CS concentration, the relatively high molecular weight (Mw = 7000) of CS also results in the excessively dense polyelectrolyte complex membrane formed on the surface of a hydrogel container and hinders the diffusion of CS. Hence, the resulting CS/SA GPM showed poor mechanical properties. Besides, increasing the molecular weights of SA can increase the mechanical properties of CS/SA GPMs. For simplicity, we chose 40 wt % CS and 1 wt % SA solutions in the following test.

To demonstrate the generality of the hydrogel-assisted reaction-diffusion method, we also chose low-cost and eco-friendly natural polysaccharide polyanions, including xanthate gum (XG), k-carrageenan (K-C), and carboxymethyl cellulose (CMC) to fabricate hydrogel-based GPMs (Figure S11a). Despite the contrasting difference in molecular structure, all these polyanions can be leveraged to construct GPMs with distinct gradient-distributed charged groups (Figure S5). The versatile material choices offer a flexible platform to regulate the mechanical properties of GPMs, as validated by Figure 2g. These results suggest that the hydrogel-assisted reaction-diffusion method is a facile and general strategy for constructing gradient ionic membranes, holding huge potential in the on-demand design of functional gradient ionic materials.

**Pressure-Sensing Performance and Mechanism.** One of the biggest merits of GPMs is to create a self-induced transmembrane potential across the GPMs due to the spontaneous diffusion of counterions driven by the concentration gradient.<sup>41–43,51,52</sup> The self-powered i-skins can be easily constructed by assembling hydrogel-based CS/SA GPMs and two metal platinum electrodes into a sandwich

configuration. When applying an increased pressure on a CS/SA GPM-based self-powered i-skin, its maximum output voltage (i.e., open-circuit voltage) decreases gradually (Figure 3a). The pressure-responsive feature of CS/SA GPM-based self-powered i-skin can be reflected by examining the pressure sensitivity, defined as  $S_p = |\Delta V / \Delta P|$ , where  $\Delta V$  and  $\Delta P$  are the variations of output voltage and applied pressure, respectively. The pressure sensitivity of self-powered i-skin is ~329.8 mV/MPa at a pressure lower than 50 kPa and decreases to 2.75 mV/MPa as the pressure increases over 200 kPa. Here, the higher sensitivity of i-skins in a low-pressure area stems from the low modulus of i-skins (Figure S12). The i-skin is also imparted with an excellent reversible response ability, even under a cyclic loading of high pressure (Figure 3b). Unlike the conventional triboelectric or piezoelectric-based electronic skins, the CS/SA GPM-based self-powered i-skin displays profound capacity in detecting the static or low-frequency dynamic mechanical stimuli (Figure 3c). Besides, the self-powered i-skins exhibit excellent durability and outstanding long-term stability. Even with a long-term incubation of up to one month, the CS/SA GPM-based self-powered i-skin can still maintain a stable electrical response under repeated loading and unloading of 5 kPa pressure for more than 500 cycles (Figure 3d and Figure S13). In addition to the CS/SA GPM, the self-powered pressure-sensing phenomena can also be achieved by many other hydrogel-based GPMs such as CS/XG, CS/K-C, and CS/CMC (Figure S11b), implying that the pressure-sensing mechanism of GPM is very generic. To highlight the advantages of GPM-based self-powered i-skins, we compared their detection limit, detection range, and durability with previously reported artificial skins. As shown in Figure S14a, the GPM-based i-skins presented a much larger detection range than others and also exhibited an ultralow detection limit and outstanding durability. Such overall performances of GPM-based i-skins are comparable to those of state-of-the-art ones. Moreover, we constructed flexible GPM-based self-powered i-skins by replacing the platinum electrode with stretchable polyacrylamide/NaCl hydrogel electrodes (Figure S15). The resulting i-skins can provide the highly precise perception of pressure variations, providing a way for one to construct bionic self-powered skins consisting entirely of ionic conductors.

To reveal the pressure-sensing mechanism of self-powered i-skins, we quantitatively analyzed the self-induced potential of hydrogel-based GPMs. Generally, owing to the gradient-distributed charged groups, there exist two kinds of ion migration within GPMs, namely, (i) spontaneous diffusion of counterions from the HD side to LD side and (ii) the internal electric field-induced ionic drifting from the LD side to HD side. The diffusion current density  $j_{\text{dif-i}}$  can be represented as

$$j_{\text{dif-i}} = -z_i F D_i \frac{dc_i}{dx} \quad (1)$$

where  $F$  is Faraday constant,  $c_i$ ,  $z_i$ , and  $D_i$  are the ionic concentration, valence, and diffusion coefficient of counterion  $i$ , respectively. The drifting current density  $j_{\text{dri-i}}$  can be described as

$$j_{\text{dri-i}} = -z_i F c_i v_i \frac{d\varphi}{dx} \quad (2)$$

$$v_i = D_i \frac{z_i F}{RT} \quad (3)$$

where  $v_i$  is mobility of counterion  $i$ , and  $\varphi$  is the self-induced potential of GPMs.  $R$  is the gas constant, and  $T$  is the temperature.

The stable transmembrane potential  $\Delta\varphi$  of GPM can be obtained when the diffusion and drifting effects reach a dynamic balance (i.e.,  $j_{\text{dif-}i} = -j_{\text{dri-}i}$ ), which can be represented as

$$\Delta\varphi = \frac{RT}{z_i F} \ln \frac{c_i(H)}{c_i(L)} \quad (4)$$

where  $c_i(H)$  and  $c_i(L)$  are concentrations of counterion  $i$  at the surfaces of the HD side and LD side, respectively. Clearly, the transmembrane potentials of GPMs are determined by the value of  $c_i(H)/c_i(L)$ . The GPMs with larger gradients can provide the larger self-induced transmembrane potentials.

Here, the GPM can be simplified as an aggregation of numerous ultrathin homogeneous layers with identical thickness, and the density of net charged groups of ultrathin layers increases gradually along the gradient/thickness direction (Figure 3e). According to eq 4, the transmembrane potential of any two adjacent ultrathin layers can be represented as follows

$$\Delta\varphi(l) = \frac{RT}{z_i F} \ln \frac{c_i(l+1)}{c_i(l)} \quad (5)$$

where  $\Delta\varphi(l)$  represents the potential difference between the middle of layers  $l$  and  $(l+1)$ , and  $c_i(l)$  and  $c_i(l+1)$  represent the concentrations of counterions at the middle of layers  $l$  and  $(l+1)$  (Figure 3e). Thus, the total transmembrane potential of GPMs can be converted into

$$\Delta\varphi = \sum_{l=1}^{n-1} \Delta\varphi(l) = \frac{RT}{F} \ln \frac{c_i(n)}{c_i(1)} \quad (6)$$

where  $n$  represents the total numbers of ultrathin layers,  $c_i(n)$  and  $c_i(1)$  represent the concentrations of counterions at the  $n$ th ultrathin layer (i.e., at the surface of HD side) and at the 1th ultrathin layer (i.e., at the surface of LD side), respectively.

When a pressure is applied on a hydrogel-based GPM, each ultrathin layer within a gradient membrane becomes thinner, and the diffusion distance of counterions is shortened. Hence, more  $\text{Na}^+$  will diffuse from the  $(l+1)$ th layer to the  $l$ th layer (or from the  $n$ th layer to the 1th layer), and the corresponding value of  $c_i(l+1)/c_i(l)$  or  $c_i(n)/c_i(1)$  decreases (Figure 3e), which results in the decrease in  $\Delta\varphi(l)$  or  $\Delta\varphi$  and thus the decrease in the output voltage of self-powered i-skins. Therefore, the low modulus is beneficial for the high pressure-sensitivity. When the water content of GPM-based i-skins is decreased by natural drying, the pressure sensitivity of i-skins decreases due to the increased compression modulus and resistance to compress stress (Figure S16a–c). Nonetheless, the i-skins can still maintain a good sensation reproducibility (Figure S16d). Similarly, with the increase of molecular weight of SA, the pressure sensitivity of CS/SA GPM-based i-skins decreases due to the increased modulus of CS/SA GPMs (Figure S10c,d). Besides, although the low modulus of CS/SA GPM prepared using  $\text{CS}_{2000}$  is beneficial for high-pressure sensitivity (Figure S10b), the  $\text{CS}_{5000}$  was utilized in the following experiments by considering both the mechanical properties and pressure sensitivity of GPMs. Furthermore, we prepared the asymmetric PAM/SA hydrogels consisting of three-layer homogeneous PAM/SA hydrogels to

simulate the hydrogel-based GPMs. The doped concentrations of SA in the bottom, middle, and top PAM/SA hydrogels are, respectively, 0.5, 1.0, and 2 wt %. In agreement with our theoretic deduction, the output voltages of as-prepared asymmetric PAM/SA hydrogels increase as the thickness of PAM/SA hydrogel monolayer increases (Figure 3f), and pressing the asymmetric PAM/SA hydrogel caused a decrease in its output voltage (Figure 3g). Such results further demonstrate the monotonous correlation between the thickness and output voltage of GPM-based self-powered i-skins. Besides, we prepared the five asymmetric three-layer PAM/SA hydrogels with different doped concentrations of SA and studied their sensing performance, as shown in Figure S17. The higher charge gradient of gradient hydrogels is beneficial for the higher pressure sensitivity. Similar results can be obtained when the ionic diodes consisting of PAM/SA and PAM/CS hydrogels were employed (Figure S18). Such results are completely different from previously reported ionic diode-based self-powered devices, whose output voltages increase under pressure. Thus, their mechanoelectric conversions should be attributed to other mechanisms.

Actually, the output potential of GPM/ionic diode-based self-powered devices is determined by both the self-induced potential of the GPM/ionic diode and the potential loss at the electrode/diode interface. Figure S19a illustrates the equivalent circuit of GPM/ionic diode-based self-powered devices. The relationship of self-induced potential and output voltage of GPM/ionic diode-based devices can thus be represented as

$$V_o = V_s - 2V_l \quad (7)$$

$$V_o = V_s - 2\frac{Q}{C_l} \quad (8)$$

where  $V_s$  and  $V_o$  are the self-induced potential of gradient hydrogel/ionic diode and output voltage of corresponding self-powered devices, respectively,  $V_l$  is the potential loss at the electrode/GPM (or electrode/diode) interface, and  $C_l$  and  $Q$  are the electrical double layer capacitance and the charge quantity at the electrode/GPM (or electrode/diode) interface, respectively. According to eqs 7 and 8, enlarging the contact area between the electrode and GPM/diode can increase the  $C_l$  and decrease the  $V_l$ , thus resulting in an increased output voltage of self-powered devices. Because of the use of nanoscale electrode materials and/or the poor connection between the ionic diode and electrodes,<sup>53</sup> pressing the previously reported diode-based devices will enlarge the  $C_l$  and hence increase their output voltages (Mechanism II in Figure S19b,c, and eq 8). This theoretical derivation is consistent with our experimental results that the output voltage of GPM/ionic diode-based self-powered i-skins increases with increasing the contact area between the electrode and GPM/diode (Figure S19d,e). In addition, we assembled a self-powered i-skin by placing two wrinkled Cu electrodes on two sides of a GPM. In agreement with our theoretical derivation, pressing the GPM-based i-skin causes the increase of output voltage due to the enlarged contact area between GPM and electrodes (Figure S19f). The results indicate that the mechanoelectric conversions of GPM/diode-based self-powered devices stem from both the thickness-dependent self-induced potentials of GPMs/ionic diodes (Mechanism I) and decreased voltage losses at the electrode/GPM or (electrode/diode) interfaces (Mechanism II) in response to pressure.

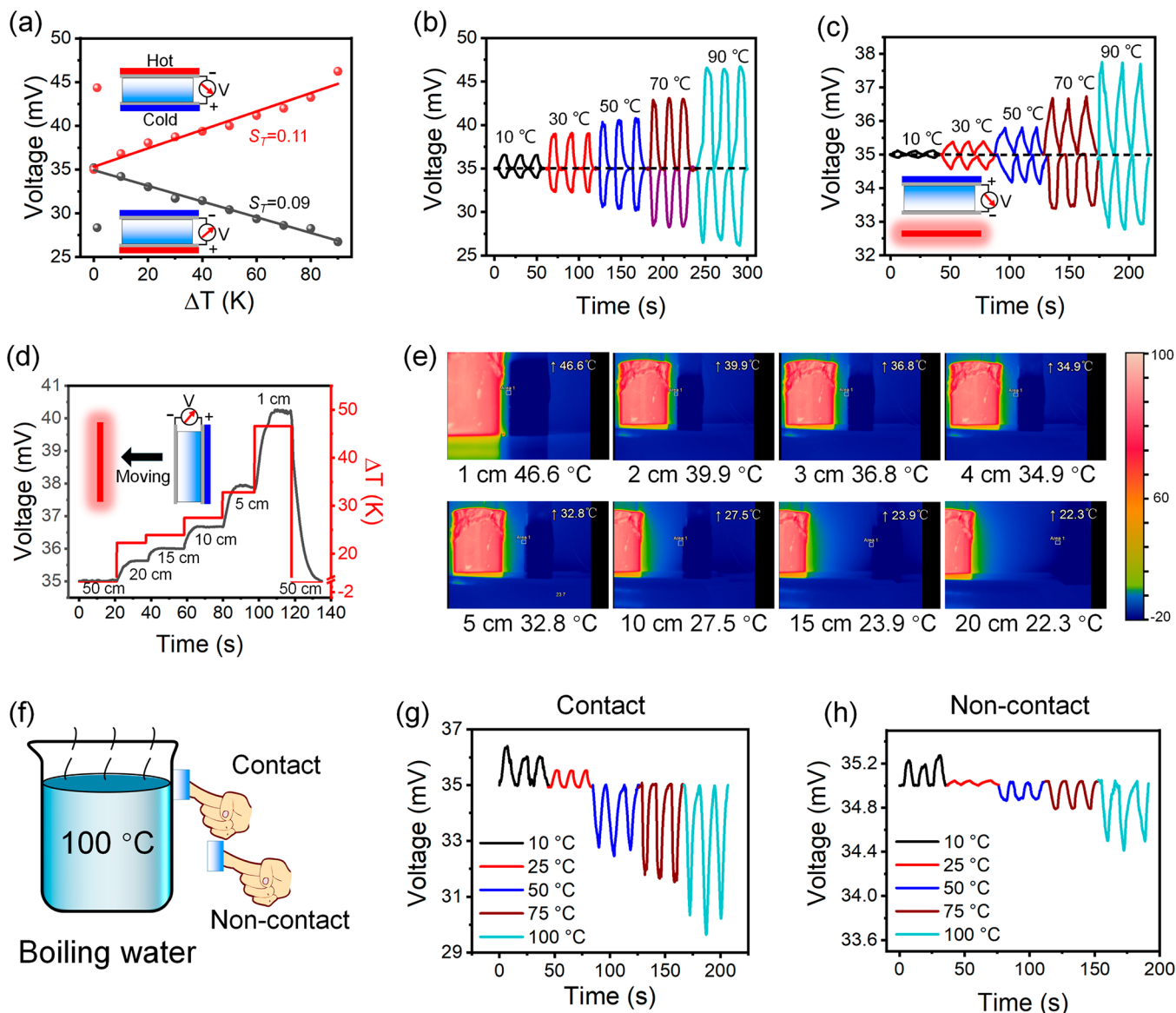


**Figure 4.** Temperature-sensing performance of self-powered i-skins. (a–d) Output voltage of self-powered i-skins under different conditions: (a) under varying temperature differences, (b) under repeated contacting with the heat sources, (c) under repeated approaches to heat sources with different temperatures, and (d) under different separation distances between the 100 °C heat source and the i-skin attached on a 0 °C container. (e) Thermal images of a self-powered i-skin attached on a 0 °C container that moved toward a 100 °C heat source gradually. (f) Schematic illustration of temperature perception of the self-powered i-skin attached on a finger in both the contact and noncontact modes. (g, h) Output voltage of self-powered i-skins attached on a finger when used to detect the temperature of heat sources in different modes: (g) contact mode and (h) noncontact mode.

The self-powered i-skins can be used to monitor a body's mechanical movement. As shown in Figure 3h, both the low-frequency walking motions ( $\sim 0.35$  Hz) and high-frequency running motions ( $\sim 1.4$  Hz) can be tracked in real time based on the variation of output voltage when the self-powered i-skins are directly attached on the heel. For the i-skin adhered to the palm, the pulse signals could be observed when the hand slapped a table (Figure S20a). Meanwhile, the high-pressure detection resolution also endows the self-powered i-skins with the ability to precisely detect subtle vibrations, such as the vocal cord vibration and periodic pulse (Figure 3i,j and Figure S20b). The distinct peaks (labeled as  $P_1$ ,  $P_2$ , and  $P_3$ ) in each period of pulse carry the comprehensive information for the human cardiovascular system, which can be used to evaluate the various physiological diseases.<sup>54</sup> Besides the pressure-

sensing function, the GPM-based self-powered devices can persistently convert the mechanical energies into electricity and, thus, work as a power supply to other devices (Figures S21 and S22).

#### Temperature-Sensing Performance and Mechanism.

When one surface of the self-powered i-skins touched a heat source, their output voltage changed due to the thermodiffusion potential stemming from the diffusion of counterions from the hot side to cold side.<sup>55</sup> Specifically, as the HD side of the self-powered i-skins touched a heat source, the output voltage increased due to the increase of net negative and positive charges at the HD side and LD side, respectively (Figure 1b and Figure 4a). Vice versa, when the LD side contacted a heat source, the output voltage of i-skins decreased. The decrement or increment (i.e.,  $|\Delta V|$ ) of the

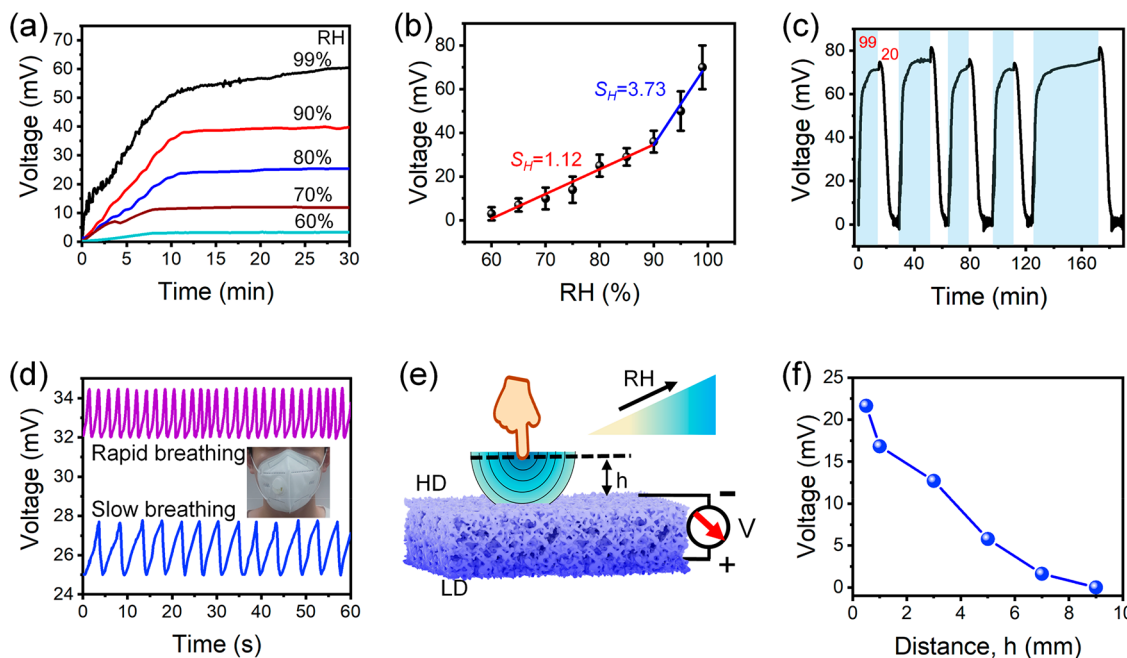


**Figure 5.** Humidity-sensing performance of self-powered i-skins. (a) Output voltage of self-powered i-skin under different RH as a function of time. (b) Humidity sensitivity of a self-powered i-skin. (c) Output voltage of a self-powered i-skin under the alternant humidity change from 99% to 20%. (d) Output voltage variation when exposed to respiration for a self-powered i-skin that settled on a commercial aspirator. (e) Schematic illustration of distance perception of a finger according to the humidity change. (f) Output voltage of self-powered i-skin when a finger moved toward it gradually.

self-powered i-skins increased with increasing the temperature difference between their two surfaces. Here, the temperature sensitivity ( $S_T = |\Delta V / \Delta T|$ ) of the self-powered i-skin is  $\sim 0.11$  and  $\sim 0.09$  mV/K when the HD side and LD side touch a heat source, respectively (Figure 4a). The temperature sensitivity increases with decreases in the water content in a hydrogel (Figure S16e), which may be attributed to the increased density of negatively charged groups and thus the increased cation selectivity.<sup>50,55,56</sup> The self-powered i-skins can provide a stable and repeatable response when repeatedly contacting the heat source with difference temperatures (Figure 4b and Figure S16f). Notably, the temperature sensitivity and response time of GPM-based i-skins are comparable to those of the state-of-the-art ones (Figure S14b).

As a little heat can change the surface temperature and create a temperature difference between their two surfaces, the self-powered i-skins can even perceive the temperature variation around a heat source in a noncontact mode. This is difficult to achieve for the reported i-skins based on the resistance signals, which are needed to be heated throughout the bodies during the test.<sup>57,58</sup> Notably, the self-powered i-skins can even perceive the temperature variation around a heat source in a noncontact mode. For instance, as the distance between the heat source and i-skin attached on a  $0\text{ }^\circ\text{C}$  container was fixed to 1 cm, the relative voltage changes of i-skin also increased with increases in the temperature of the heat source (Figure 4c). This is attributed to the enhanced thermal radiation intensity around the heat source, which increased the temperature difference between two surfaces of the i-skin (Figure S23). The self-powered i-skins could be used to capture the temperature distribution of a heat source (Figure S24). When the i-skin moved toward a  $100\text{ }^\circ\text{C}$  heat source, the relative voltage change increased due to the increased thermal radiation intensity (or environmental

temperature around the heat source). A stepwise increase of output voltage could be observed as the i-skins approached the heat source step by step (Figure 4d). An infrared thermal imager was used to capture the temperature change of the self-powered i-skins during the moving (Figure 4e). It suggests that a small temperature change (1.6 K) induced by heat radiation can give rise to a recognizable voltage change of the i-skins.

The self-powered i-skin fixed on the palm could be utilized to precisely perceive the temperature of heat sources in both the contact and noncontact modes (Figure 4f-h and Figure S25). This means that we can deduce the true temperature of the heat source according to the temperature distribution around it that was captured in the noncontact perception mode. This can avoid the burn of skins in the case of the overtemperature of heat sources as well as allow one to access diverse applications such as touchless control and contact warning.

Additionally, the hydrated GPM-based self-powered i-skins can distinguish the voltage changes caused by pressure stimulation and thermodiffusion according to distinctive waveforms of voltage signals derived from pressure and temperature stimuli. Under the external pressure, the output voltage of GPM-based i-skin decreased sharply to a constant value (Figure 3b), while its output voltage gradually evolved to the equilibrium value using  $\sim 10$  s upon the trigger of temperature difference (Figure 4b). When exposed to the pressure and temperature stimuli simultaneously, the changed voltage signals of GPM-based self-powered i-skins can be divided into two parts, namely, the abruptly decreased voltage signals stemming from the pressure ( $\Delta V_p$ ) and gradual changed voltage signals induced by the thermodiffusion ( $\Delta V_T$ , Figure S26a-f). Figure S26g-i shows the total voltage,  $\Delta V_p$ , and  $\Delta V_T$  of a self-powered i-skin in response to the combination of pressure and temperature stimuli. Clearly, the

i-skins present the analogical  $\Delta V_T$  at the same temperature under different pressures (Figure S26d,e,i) and the similar  $\Delta V_P$  at the same pressure under different temperature differences (Figure S26f,h). Such results demonstrate the feasibility of using GPM-based self-powered i-skins to distinguish the voltage changes caused by pressure stimulation and thermodiffusion.

**Humidity-Sensing Performance.** To extend the application scope of the self-powered i-skins in humidity sensors, we leveraged a freeze-dried technology to improve the response ability of CS/SA GPMs in moisture (Figure 5). When exposed to the moisture, a gradual increased self-induced voltage of the i-skin could be observed due to the gradual hydration of polar groups and the spontaneous diffusion of counterions, which can be stabilized within  $\sim 10$  min (Figure 5a). The maximum output voltage of i-skins increased with the increase of humidity. This is attributed to increased ionized and diffused degrees of counterions in response to high humidity.<sup>39–43</sup> A step-by-step increase in humidity resulted in a stepwise increased voltage signal (Figure S27). The humidity sensitivity of a freeze-dried self-powered i-skin is  $\sim 1.12$  mV/RH% at a low humidity (relative humidity (RH) < 90%) and increases to  $\sim 3.73$  mV/RH% when the humidity is higher than 90% (Figure 5b). The self-induced potential could return to the initial state when the i-skins were placed in a dried environment for  $\sim 12$  min (RH = 20%, Figure 5c). The sensitivity can be further improved to 2.05 mV/RH% by modifying the GPMs (Figure S28). When integrated with a commercial respirator, the freeze-dried i-skin could detect the frequency and intensity of dynamic breathing (Figure 5d). Besides, the freeze-dried i-skins could perceive the distance away from the skins based on the distance-determined moisture distribution near the human skin (Figure 5e). When a finger moved toward a self-powered i-skin gradually, the output voltage of the i-skin increased accordingly (Figure 5f).

## CONCLUSION

In summary, we have demonstrated that the GPMs can be directly used as self-powered i-skins for the precise perception of multiple stimuli (i.e., pressure, temperature, and humidity). The GPMs are prepared by a yet versatile hydrogel-assisted reaction-diffusion method. It has been proved that gradient-distributed charged groups of GPMs enable one to generate a thickness-dependent and thermoresponsive self-induced potential on hydrated GPMs as well as a humidity-sensitive self-induced potential on dehydrated/dried GPMs, respectively. Therefore, the GPM-based self-powered i-skin gradient membranes can provide a highly sensitive and reliable detection of external pressure, temperature, and humidity based on the potential signals. The resulting self-powered i-skins enable the high-precision monitoring of human activities and can precisely perceive the temperature distribution in the surrounding environment in a noncontact mode. Moreover, we have revealed the mechanoelectric conversion/sensing mechanism of GPM/ionic diode-based self-powered i-skins. This work provides a path to construct high-performance self-powered i-skins as well as to develop a general strategy for the fast fabrication of large-scale asymmetric polyelectrolyte membranes.

## METHODS

**Materials.** HMW SA (Mw = 388 000) was provided by Qingdao Hyzlin Biology Development Co., Ltd. LMW CS (Mw = 5000) with a 90% degree of deacetylation was purchased from Weifang Dongxing Carapace Products Factory. XG, K–C, CMC, acrylamide (AM, >98%), N,N'-methylenebis(acrylamide) (BIS, 98%), ammonium peroxodisulfate (APS, 99.99%) N,N,N',N'-tetramethylethylene-diamine (TEMED, 96%), and NaCl (99.9%) were purchased from Aladdin Reagents Co., Ltd. Platinum sheet electrodes were purchased from Shanghai Yueci Electronic Technology Co., Ltd. The Pt mesh (mesh size  $\approx 0.25$  mm, 0.12 mm in diameter) electrodes were purchased from Beijing Global Jinxin International Technology Co., Ltd. Deionized water with a resistivity of  $18.2\text{ M}\Omega\text{ cm}^{-1}$  was used in all experiments.

**Preparation of Polyacrylamide Hydrogel Containers.** The PAM hydrogels were used as the LWM polycation containers, which were prepared by a thermo-induced radical polymerization. In brief, AM (monomer, 20 g) and BIS (cross-linker, 34.5 mg) were added into 80 mL of distilled water. After this was stirred for 0.5 h, APS (initiator, 0.032 g) and TEMED (accelerator, 80  $\mu\text{L}$ ) were added to the solution under an ice bath. The mixture was treated by ultrasonic waves for 2 min in ice water and injected into the sealed molds with various configurations. After thermopolymerization in an oven at 50 °C for 2 h, the PAM hydrogel containers were obtained.

**Preparation of GPMs.** The as-prepared hydrogel container was first immersed in a CS solution (40 wt %) for 12 h and then submerged into sufficient HMW-SA solution (1 wt %). The hydrogel-based CS/SA GPMs were formed directly on the surface of PAM hydrogel containers with an adjustable thickness that increased with the reaction time. The CS/XG, CS/K–C, and CS/CMC GPMs were prepared by the same method. We note that the AM monomers cannot be polymerized to form continuous hydrogel networks in the concentrated LMW CS solution. Hence an immersion process was employed to prepare LMW CS/PAM hydrogels.

**Preparation of Self-Powered i-Skins.** The self-powered i-skins were integrated readily by connecting upper and lower sides of the hydrogel-based GPMs to two Pt electrodes, respectively. For humidity sensing, the freeze-dried GPMs and platinum mesh electrodes were used without covering tape. During the experiments, the GPM-based self-powered i-skins were attached on the tested solid surfaces by a commercial biaxially oriented polypropylene (BOPP) tape and/or copper foil tapes. For the long-term test or the test at high temperatures, the GPM-based self-powered i-skins were encapsulated into commercial polyimide tapes.

**Characterizations.** The cross-section morphologies of GPMs were observed by a field-emission scanning electron microscope (JSM 7800F) operating at 10 kV. The charge distributions of the GPMs were analyzed through a confocal laser scanning microscope (Axiomager LSM-800). The membranes were dyed by the dilute solution of positively charged rhodamine 6G ( $10^{-6}$  M) for  $\sim 24$  h. The chemical structures of the GPMs were characterized using an attenuated total reflection mode FTIR (Nicolet iSS0) and an X-ray photoelectron spectrometer (EscaLab Xi+). The zeta potential was tested by Malvern Zetasizer (Nano ZSE). The mechanical properties were characterized with the strip-like hydrogel-based GPMs using a testing machine (WDW-ST) at a compression and tensile speed of 5 mm/min. The elastic modulus ( $E$ ),  $E = \sigma/\epsilon$ , was calculated from the stress and strain between  $\epsilon = 10\%-30\%$ . The temperature distributions of the samples were tested by an infrared thermal imager (Fluke, Ti480 PRO). The pore size distribution was determined by the Brunauer–Emmett–Teller (BET)  $N_2$  adsorption/desorption method (ASAP 2420) and Brunauer–Joyner–Hallenda (BJH) method using desorption data. The pore size distribution was also measured by a mercury intrusion method (Micromeritics AutoPore V 9620). The molecular weights of SA and CS were determined by gel permeation chromatography (Agilent 1260). The electrical signal measurements of self-powered i-skins were conducted with a Keithley 2450 digital meter.

## ASSOCIATED CONTENT

### Supporting Information

The Supporting Information is available free of charge at <https://pubs.acs.org/doi/10.1021/acsnano.1c11505>.

UV-Vis transmittance spectra, FTIR measurements, BET test, mercury intrusion porosimetry test, XPS spectra, Zeta potential, SEM images, optical images, thermal images, stress-strain curves of the GPMs, sensing performance, sensing mechanism of GPMs-based i-skins, comparisons between the i-skins and other sensors, structural formulas and sources of other polyelectrolytes, and optical images of hydrogel containers and corresponding GPMs ([PDF](#))

## AUTHOR INFORMATION

### Corresponding Authors

Wenxin Fan — College of Materials Science and Engineering, State Key Laboratory of Bio-fibers and Eco-textiles, Shandong Collaborative Innovation Center of Marine Biobased Fibers and Ecological Textiles, Qingdao University, Qingdao 266071, P. R. China; Email: [fanwenxin@qdu.edu.cn](mailto:fanwenxin@qdu.edu.cn)

Zuankai Wang — Department of Mechanical Engineering, City University of Hong Kong, Hong Kong 999077, P. R. China; [orcid.org/0000-0002-3510-1122](https://orcid.org/0000-0002-3510-1122); Email: [zuanwang@cityu.edu.hk](mailto:zuanwang@cityu.edu.hk)

Kunyan Sui — College of Materials Science and Engineering, State Key Laboratory of Bio-fibers and Eco-textiles, Shandong Collaborative Innovation Center of Marine Biobased Fibers and Ecological Textiles, Qingdao University, Qingdao 266071, P. R. China; [orcid.org/0000-0001-9143-0767](https://orcid.org/0000-0001-9143-0767); Email: [sky@qdu.edu.cn](mailto:sky@qdu.edu.cn)

### Authors

Mingyang Xia — College of Materials Science and Engineering, State Key Laboratory of Bio-fibers and Eco-textiles, Shandong Collaborative Innovation Center of Marine Biobased Fibers and Ecological Textiles, Qingdao University, Qingdao 266071, P. R. China

Na Pan — College of Materials Science and Engineering, State Key Laboratory of Bio-fibers and Eco-textiles, Shandong Collaborative Innovation Center of Marine Biobased Fibers and Ecological Textiles, Qingdao University, Qingdao 266071, P. R. China

Chao Zhang — Department of Mechanical Engineering, City University of Hong Kong, Hong Kong 999077, P. R. China; [orcid.org/0000-0002-1275-7794](https://orcid.org/0000-0002-1275-7794)

Chengjing Zhang — College of Materials Science and Engineering, State Key Laboratory of Bio-fibers and Eco-textiles, Shandong Collaborative Innovation Center of Marine Biobased Fibers and Ecological Textiles, Qingdao University, Qingdao 266071, P. R. China

Yanzhi Xia — College of Materials Science and Engineering, State Key Laboratory of Bio-fibers and Eco-textiles, Shandong Collaborative Innovation Center of Marine Biobased Fibers and Ecological Textiles, Qingdao University, Qingdao 266071, P. R. China

Complete contact information is available at:

<https://pubs.acs.org/10.1021/acsnano.1c11505>

### Author Contributions

<sup>§</sup>M.-Y.X. and N.P. contributed equally to this work. Y.-Z.X. and K.-Y.S. proposed and supervised the project. M.-Y.X. and W.-X.F.

X.F. conceived and designed the experiments. M.-Y.X., N.P., and W.-X.F. performed the experiments and analyzed the data. C.Z. and Z.-K.W. gave guidance on the data analysis and paper revision. C.-J.Z. helped to perform some experiments and analyze the data. M.-Y.X., N.P., W.-X.F., Z.-K.W., and K.-Y.S. cowrote the manuscript.

### Notes

The authors declare no competing financial interest.

## ACKNOWLEDGMENTS

This work was supported by the National Natural Science Foundation of China (51573080, 52003133, and 51873094), the Key Research and Development Project of Shandong Province (2016GGX102005), the Technology Development Project of Shinan District of Qingdao (2018-4-007-ZH), and Program for Taishan Scholar of Shandong Province.

## REFERENCES

- (1) Chou, H. H.; Nguyen, A.; Chortos, A.; To, J. W.; Lu, C.; Mei, J.; Kurosawa, T.; Bae, W. G.; Tok, J. B.; Bao, Z. A Chameleon-Inspired Stretchable Electronic Skin with Interactive Colour Changing Controlled by Tactile Sensing. *Nat. Commun.* **2015**, *6*, 8011.
- (2) Wu, Y.; Liu, Y.; Zhou, Y.; Man, Q.; Hu, C.; Asghar, W.; Li, F.; Yu, Z.; Shang, J.; Liu, G.; Liao, M.; Li, R. W. A Skin-Inspired Tactile Sensor for Smart Prosthetics. *Sci. Robot.* **2018**, *3*, eaat0429.
- (3) Ikeda, R.; Cha, M.; Ling, J.; Jia, Z.; Coyle, D.; Gu, J. G. Merkel Cells Transduce and Encode Tactile Stimuli to Drive  $\text{A}\beta$ -Afferent Impulses. *Cell* **2014**, *157*, 664–675.
- (4) Lee, S.; Franklin, S.; Hassani, F. A.; Yokota, T.; Nayem, M. O. G.; Wang, Y.; Leib, R.; Cheng, G.; Franklin, D. W.; Someya, T. Nanomesh Pressure Sensor for Monitoring Finger Manipulation without Sensory Interference. *Science* **2020**, *370*, 966–970.
- (5) Ray, T. R.; Choi, J.; Bandodkar, A. J.; Krishnan, S.; Gutruf, P.; Tian, L.; Ghaffari, R.; Rogers, J. A. Bio-Integrated Wearable Systems: A Comprehensive Review. *Chem. Rev.* **2019**, *119*, 5461–5533.
- (6) Yang, C. H.; Suo, Z. G. Hydrogel Iontronics. *Nat. Rev. Mater.* **2018**, *3*, 125–142.
- (7) Chortos, A.; Liu, J.; Bao, Z. Pursuing Prosthetic Electronic Skin. *Nat. Mater.* **2016**, *15*, 937–950.
- (8) Chao, M.; He, L.; Gong, M.; Li, N.; Li, X.; Peng, L.; Shi, F.; Zhang, L.; Wan, P. Breathable  $\text{Ti}_3\text{C}_2\text{T}_{\text{x}}$  MXene/Protein Nanocomposites for Ultrasensitive Medical Pressure Sensor with Degradability in Solvents. *ACS Nano* **2021**, *15*, 9746–9758.
- (9) Wang, C.; Pan, C.; Wang, Z. Electronic Skin for Closed-Loop Systems. *ACS Nano* **2019**, *13*, 12287–12293.
- (10) Lei, Z.; Wu, P. Zwitterionic Skins with a Wide Scope of Customizable Functionalities. *ACS Nano* **2018**, *12*, 12860–12868.
- (11) Zhang, X. H.; Sheng, N. N.; Wang, L. A.; Tan, Y. Q.; Liu, C. Z.; Xia, Y. Z.; Nie, Z. H.; Sui, K. Y. Supramolecular Nanofibrillar Hydrogels as Highly Stretchable, Elastic and Sensitive Ionic Sensors. *Mater. Horiz.* **2019**, *6*, 326–333.
- (12) Sun, J. Y.; Keplinger, C.; Whitesides, G. M.; Suo, Z. Ionic Skin. *Adv. Mater.* **2014**, *26*, 7608–7614.
- (13) Fan, W.; Shan, C.; Guo, H.; Sang, J.; Wang, R.; Zheng, R.; Sui, K.; Nie, Z. Dual-Gradient Enabled Ultrafast Biomimetic Snapping of Hydrogel Materials. *Sci. Adv.* **2019**, *5*, eaav7174.
- (14) Chang, Y.; Wang, L.; Li, R.; Zhang, Z.; Wang, Q.; Yang, J.; Guo, C. F.; Pan, T. First Decade of Interfacial Iontronic Sensing: From Droplet Sensors to Artificial Skins. *Adv. Mater.* **2021**, *33*, e2003464.
- (15) Bai, N.; Wang, L.; Wang, Q.; Deng, J.; Wang, Y.; Lu, P.; Huang, J.; Li, G.; Zhang, Y.; Yang, J.; Xie, K.; Zhao, X.; Guo, C. F. Graded Intrafillable Architecture-Based Iontronic Pressure Sensor with Ultra-Broad-Range High Sensitivity. *Nat. Commun.* **2020**, *11*, 209.
- (16) Wu, X.; Ahmed, M.; Khan, Y.; Payne, M. E.; Zhu, J.; Lu, C.; Evans, J. W.; Arias, A. C. A Potentiometric Mechanotransduction Mechanism for Novel Electronic Skins. *Sci. Adv.* **2020**, *6*, eaba1062.

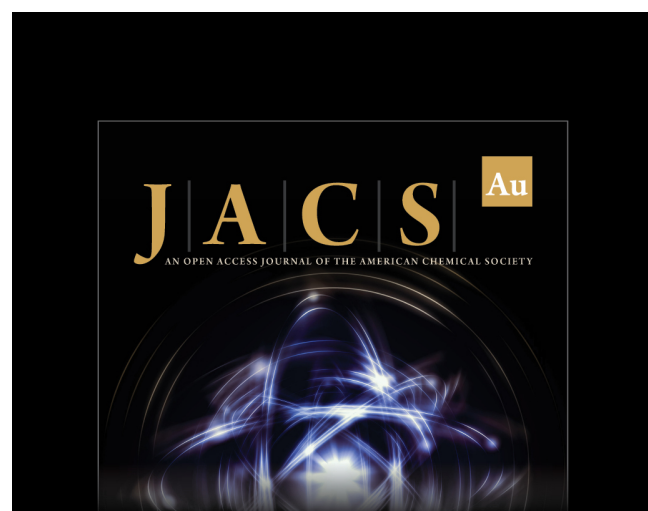
- (17) Zhang, D.; Qiao, H.; Fan, W.; Zhang, K.; Xia, Y.; Sui, K. Self-Powered Ionic Sensors Overcoming the Limitation of Ionic Conductors as Wearable Sensing Devices. *Mater. Today Phys.* **2020**, *15*, 100246.
- (18) You, I.; Mackanic, D. G.; Matsuhsisa, N.; Kang, J.; Kwon, J.; Beker, L.; Mun, J.; Suh, W.; Kim, T. Y.; Tok, J. B.; Bao, Z.; Jeong, U. Artificial Multimodal Receptors Based on Ion Relaxation Dynamics. *Science* **2020**, *370*, 961–965.
- (19) Lei, Z.; Wu, P. A Highly Transparent and Ultra-Stretchable Conductor with Stable Conductivity During Large Deformation. *Nat. Commun.* **2019**, *10*, 3429.
- (20) Ren, Y.; Liu, Z.; Jin, G.; Yang, M.; Shao, Y.; Li, W.; Wu, Y.; Liu, L.; Yan, F. Electric-Field-Induced Gradient Ionogels for Highly Sensitive, Broad-Range-Response, and Freeze/Heat-Resistant Ionic Fingers. *Adv. Mater.* **2021**, *33*, 2008486.
- (21) Zhang, C.; Wu, B.; Zhou, Y.; Zhou, F.; Liu, W.; Wang, Z. Mussel-Inspired Hydrogels: from Design Principles to Promising Applications. *Chem. Soc. Rev.* **2020**, *49*, 3605–3637.
- (22) Yu, Z.; Wu, P. Underwater Communication and Optical Camouflage Ionogels. *Adv. Mater.* **2021**, *33*, 2008479.
- (23) Gao, G.; Yang, F.; Zhou, F.; He, J.; Lu, W.; Xiao, P.; Yan, H.; Pan, C.; Chen, T.; Wang, Z. L. Bioinspired Self-Healing Human-Machine Interactive Touch Pad with Pressure-Sensitive Adhesiveness on Targeted Substrates. *Adv. Mater.* **2020**, *32*, 2004290.
- (24) Li, S.; Pan, N.; Zhu, Z.; Li, R.; Li, B.; Chu, J.; Li, G.; Chang, Y.; Pan, T. All-in-One Iontronic Sensing Paper. *Adv. Funct. Mater.* **2019**, *29*, 1807343.
- (25) Wang, Y.; Cao, X.; Cheng, J.; Yao, B.; Zhao, Y.; Wu, S.; Ju, B.; Zhang, S.; He, X.; Niu, W. Cephalopod-Inspired Chromotropic Ionic Skin with Rapid Visual Sensing Capabilities to Multiple Stimuli. *ACS Nano* **2021**, *15*, 3509–3521.
- (26) Yeom, J.; Choe, A.; Lim, S.; Lee, Y.; Na, S.; Ko, H. Soft and Ion-Conducting Hydrogel Artificial Tongue for Astringency Perception. *Sci. Adv.* **2020**, *6*, eaba5785.
- (27) Lee, Y.; Cha, S. H.; Kim, Y. W.; Choi, D.; Sun, J. Y. Transparent and Attachable Ionic Communicators Based on Self-Cleanable Triboelectric Nanogenerators. *Nat. Commun.* **2018**, *9*, 1804.
- (28) Pu, X.; Liu, M.; Chen, X.; Sun, J.; Du, C.; Zhang, Y.; Zhai, J.; Hu, W.; Wang, Z. L. Ultrastretchable, Transparent Triboelectric Nanogenerator as Electronic Skin for Biomechanical Energy Harvesting and Tactile Sensing. *Sci. Adv.* **2017**, *3*, e1700015.
- (29) Liu, T.; Liu, M.; Dou, S.; Sun, J.; Cong, Z.; Jiang, C.; Du, C.; Pu, X.; Hu, W.; Wang, Z. L. Triboelectric-Nanogenerator-Based Soft Energy-Harvesting Skin Enabled by Toughly Bonded Elastomer/Hydrogel Hybrids. *ACS Nano* **2018**, *12*, 2818–2826.
- (30) Lai, Y. C.; Wu, H. M.; Lin, H. C.; Chang, C. L.; Chou, H. H.; Hsiao, Y. C.; Wu, Y. C. Entirely, Intrinsically, and Autonomously Self-Healable, Highly Transparent, and Superstretchable Triboelectric Nanogenerator for Personal Power Sources and Self-Powered Electronic Skins. *Adv. Funct. Mater.* **2019**, *29*, 1904626.
- (31) Fu, R. M.; Tu, L. J.; Zhou, Y. H.; Fan, L.; Zhang, F. M.; Wang, Z. G.; Xing, J.; Chen, D. F.; Deng, C. L.; Tan, G. X.; Yu, P.; Zhou, L.; Ning, C. Y. A Tough and Self-Powered Hydrogel for Artificial Skin. *Chem. Mater.* **2019**, *31*, 9850–9860.
- (32) Zhang, S.; Wang, Y.; Yao, X.; Le Floch, P.; Yang, X.; Liu, J.; Suo, Z. Stretchable Electrets: Nanoparticle-Elastomer Composites. *Nano Lett.* **2020**, *20*, 4580–4587.
- (33) Wang, Z. L.; Wang, A. C. On the Origin of Contact-Electrification. *Mater. Today* **2019**, *30*, 34–51.
- (34) Kim, H. J.; Chen, B.; Suo, Z.; Hayward, R. C. Ionoelastomer Junctions between Polymer Networks of Fixed Anions and Cations. *Science* **2020**, *367*, 773–776.
- (35) Hou, Y.; Zhou, Y.; Yang, L.; Li, Q.; Zhang, Y.; Zhu, L.; Hickner, M. A.; Zhang, Q.; Wang, Q. Flexible Ionic Diodes for Low-Frequency Mechanical Energy Harvesting. *Adv. Energy Mater.* **2017**, *7*, 1601983.
- (36) Ying, B. B.; Wu, Q. Y.; Li, J. Y.; Liu, X. Y. An Ambient-Stable and Stretchable Ionic Skin with Multimodal Sensation. *Mater. Horiz.* **2020**, *7*, 477–488.
- (37) Vermaas, D. A.; Saakes, M.; Nijmeijer, K. Doubled Power Density from Salinity Gradients at Reduced Intermembrane Distance. *Environ. Sci. Technol.* **2011**, *45*, 7089–7095.
- (38) Zhang, Z.; Kong, X. Y.; Xiao, K.; Xie, G.; Liu, Q.; Tian, Y.; Zhang, H.; Ma, J.; Wen, L.; Jiang, L. A Bioinspired Multifunctional Heterogeneous Membrane with Ultrahigh Ionic Rectification and Highly Efficient Selective Ionic Gating. *Adv. Mater.* **2016**, *28*, 144–150.
- (39) Zhu, X.; Hao, J.; Bao, B.; Zhou, Y.; Zhang, H.; Pang, J.; Jiang, Z.; Jiang, L. Unique ion rectification in hypersaline environment: A High-Performance and Sustainable Power Generator System. *Sci. Adv.* **2018**, *4*, eaau1665.
- (40) Guo, W.; Tian, Y.; Jiang, L. Asymmetric Ion Transport Through Ion-Channel-Mimetic Solid-State Nanopores. *Acc. Chem. Res.* **2013**, *46*, 2834–2846.
- (41) Sun, Z.; Feng, L.; Wen, X.; Wang, L.; Qin, X.; Yu, J. Nanofiber Fabric Based Ion-Gradient-Enhanced Moist-Electric Generator with a Sustained Voltage Output of 1.1 V. *Mater. Horiz.* **2021**, *8*, 2303–2309.
- (42) Yang, W. Q.; Li, X. K.; Han, X.; Zhang, W. H.; Wang, Z. B.; Ma, X. M.; Li, M. J.; Li, C. X. Asymmetric Ionic Aerogel of Biologic Nanofibrils for Harvesting Electricity from Moisture. *Nano Energy* **2020**, *71*, 104610.
- (43) Zhao, F.; Cheng, H.; Zhang, Z.; Jiang, L.; Qu, L. Direct Power Generation from a Graphene Oxide Film under Moisture. *Adv. Mater.* **2015**, *27*, 4351–4357.
- (44) Cui, H.; Pan, N.; Fan, W.; Liu, C.; Li, Y.; Xia, Y.; Sui, K. Ultrafast Fabrication of Gradient Nanoporous All-Polysaccharide Films as Strong, Superfast, and Multiresponsive Actuators. *Adv. Funct. Mater.* **2019**, *29*, 1807692.
- (45) Pan, N.; Lin, M.; Cui, H.; Fan, W.; Liu, C.; Chen, F.; Fan, C.; Xia, Y.; Sui, K. Accurate Control of All-Polymer Hollow Multishelled Spheres by One-Step Reaction-Diffusion. *Chem. Mater.* **2020**, *32*, 8442–8449.
- (46) Su, X.; Xie, W.; Wang, P.; Tian, Z.; Wang, H.; Yuan, Z.; Liu, X.; Huang, J. Strong Underwater Adhesion of Injectable Hydrogels Triggered by Diffusion of Small Molecules. *Mater. Horiz.* **2021**, *8*, 2199–2207.
- (47) Wang, H.; Su, X.; Chai, Z.; Tian, Z.; Xie, W.; Wang, Y.; Wan, Z.; Deng, M.; Yuan, Z.; Huang, J. A Hydra Tentacle-Inspired Hydrogel with Underwater Ultra-Stretchability for Adhering Adipose Surfaces. *Chem. Eng. J.* **2022**, *428*, 131049.
- (48) Bian, G.; Pan, N.; Luan, Z.; Sui, X.; Fan, W.; Xia, Y.; Sui, K.; Jiang, L. Anti-Swelling Gradient Polyelectrolyte Hydrogel Membranes as High-Performance Osmotic Energy Generators. *Angew. Chem., Int. Ed.* **2021**, *60*, 20294–20300.
- (49) Li, Y.; Pan, N.; Lin, M.; Liu, Y.; Yan, W.; Cui, X.; Xia, Y.; Sui, K. Building Nano-Thin Shells for All-Polymer Hollow Multishelled Spheres: Rigidity and Reaction-Shrinkage of Composite Network. *Compos. Commun.* **2021**, *28*, 100920.
- (50) Zhang, Z.; He, L.; Zhu, C.; Qian, Y.; Wen, L.; Jiang, L. Improved Osmotic Energy Conversion in Heterogeneous Membrane Boosted by Three-Dimensional Hydrogel Interface. *Nat. Commun.* **2020**, *11*, 875.
- (51) Wang, H.; Sun, Y.; He, T.; Huang, Y.; Cheng, H.; Li, C.; Xie, D.; Yang, P.; Zhang, Y.; Qu, L. Bilayer of Polyelectrolyte Films for Spontaneous Power Generation in Air up to an Integrated 1,000 V Output. *Nat. Nanotechnol.* **2021**, *16*, 811–819.
- (52) Huang, Y.; Cheng, H.; Yang, C.; Zhang, P.; Liao, Q.; Yao, H.; Shi, G.; Qu, L. Interface-Mediated Hygroelectric Generator with an Output Voltage Approaching 1.5 V. *Nat. Commun.* **2018**, *9*, 4166.
- (53) Zhang, Y.; Jeong, C. K.; Wang, J.; Chen, X.; Choi, K. H.; Chen, L. Q.; Chen, W.; Zhang, Q. M.; Wang, Q. Hydrogel Ionic Diodes toward Harvesting Ultralow-Frequency Mechanical Energy. *Adv. Mater.* **2021**, *33*, e2103056.
- (54) Wang, Y.; Gong, S.; Wang, S. J.; Simon, G. P.; Cheng, W. L. Volume-Invariant Ionic Liquid Microbands as Highly Durable Wearable Biomedical Sensors. *Mater. Horiz.* **2016**, *3*, 208–213.

(55) Han, C. G.; Qian, X.; Li, Q.; Deng, B.; Zhu, Y.; Han, Z.; Zhang, W.; Wang, W.; Feng, S. P.; Chen, G.; Liu, W. Giant Thermopower of Ionic Gelatin Near Room Temperature. *Science* **2020**, *368*, 1091–1098.

(56) Liu, C.; Li, Q.; Wang, S.; Liu, W.; Fang, N. X.; Feng, S.-P. Ion Regulation in Double-Network Hydrogel Module with Ultrahigh Thermopower for Low-Grade Heat Harvesting. *Nano Energy* **2022**, *92*, 106738.

(57) Ge, G.; Lu, Y.; Qu, X.; Zhao, W.; Ren, Y.; Wang, W.; Wang, Q.; Huang, W.; Dong, X. Muscle-Inspired Self-Healing Hydrogels for Strain and Temperature Sensor. *ACS Nano* **2020**, *14*, 218–228.

(58) Guo, H.; Bai, M.; Zhu, Y.; Liu, X.; Tian, S.; Long, Y.; Ma, Y.; Wen, C.; Li, Q.; Yang, J.; Zhang, L. Pro-Healing Zwitterionic Skin Sensor Enables Multi-Indicator Distinction and Continuous Real-Time Monitoring. *Adv. Funct. Mater.* **2021**, *31*, 2102406.



The image shows the front cover of the journal *JACS Au*. The title "JACS" is prominently displayed in large, gold-colored letters, with "Au" in a smaller square to the right. Below the title, it says "AN OPEN ACCESS JOURNAL OF THE AMERICAN CHEMICAL SOCIETY". The background features a dark, abstract graphic of glowing blue and white lines forming a complex, swirling pattern.

Editor-in-Chief  
**Prof. Christopher W. Jones**  
Georgia Institute of Technology, USA

**Open for Submissions** 

pubs.acs.org/jacsau ACS Publications  
Most Trusted. Most Cited. Most Read.